Structure 14, 21–31, January 2006 ©2006 Elsevier Ltd All rights reserved DOI 10.1016/j.str.2005.09.018

The Structure of the N-Terminal Domain of the Fragile X Mental Retardation Protein: A Platform for Protein-Protein Interaction

Andres Ramos,[1] David Hollingworth,[1] Salvatore Adinolfi,[1] Marie Castets,[3] Geoff Kelly,[2] Thomas A. Frenkiel,[2] Barbara Bardoni,[4] and Annalisa Pastore[1,*]

[1]Molecular Structure Division
[2]Biomedical NMR Centre
National Institute for Medical Research
London, NW7 1AA
United Kingdom
[3]IGBMC
CNRS/INSERM/ULP
BP 10142
1 rue Laurent Fries
67404 Illkirch
France
[4]Faculté de Medicine
CNRS FRE 2720
Avenue Valombrose
06107 Nice
France

Summary

FMRP, whose lack of expression causes the X-linked fragile X syndrome, is a modular RNA binding protein thought to be involved in posttranslational regulation. We have solved the structure in solution of the *N*-terminal *d*omain of *F*MRP (NDF), a functionally important region involved in multiple interactions. The structure consists of a composite fold comprising two repeats of a Tudor motif followed by a short α helix. The interactions between the three structural elements are essential for the stability of the NDF fold. Although structurally similar, the two repeats have different dynamic and functional properties. The second, more flexible repeat is responsible for interacting both with methylated lysine and with 82-FIP, one of the FMRP nuclear partners. NDF contains a 3D nucleolar localization signal, since destabilization of its fold leads to altered nucleolar localization of FMRP. We suggest that the NDF composite fold determines an allosteric mechanism that regulates the FMRP functions.

Introduction

Absence of the *f*ragile X *m*ental *r*etardation *p*rotein (FMRP) causes the fragile X syndrome, the most common form of inherited mental retardation in humans (Bardoni et al., 1999). FMRP is a predominantly cytoplasmic, multidomain protein that is particularly abundant in neurons, where it is involved in nuclear export, stability, and localization of a subpopulation of mRNAs in the dendrites (Brown et al., 2001; Schaeffer et al., 2001; Darnell et al., 2001; Keene and Tenenbaum, 2002), and functions as a negative regulator of translation (Li et al., 2001; Laggerbauer et al., 2001; Mazroui et al., 2002; Zalfa et al., 2003).

FMRP has a complex functional cycle. After its synthesis in the cytoplasm, the protein moves into the nucleus and associates with several other proteins, with RNAs, and, possibly, with ribosomes (Jin and Warren, 2003). It is then exported to the cytoplasm where it is detected in the context of the large ribosome-containing RNP particles that migrate along the dendritic axis to reach the neural synapses (De Diego Otero et al., 2002). Lack of functional FMRP affects the assembly of RNP particles (Mazroui et al., 2002) and the regulation of translation of several mRNAs (D'Agata et al., 2002; Chen et al., 2003), leading to abnormal synapses (Zhang et al., 2001).

The functions of FMRP in different cellular compartments are mediated by its interaction with RNA (Brown et al., 2001; Schaeffer et al., 2001; Darnell et al., 2001; Zalfa et al., 2003; Jin and Warren, 2003) and with several protein partners (Ceman et al., 1999, 2000; Bardoni and Mandel, 2002; Bardoni et al., 2003; Caudy et al., 2002; Ishizuka et al., 2002). Interestingly, many of these protein-protein interactions have been mapped onto the amino terminus of the protein where an independently folded domain, termed NDF (for N-terminal domain of FMRP), was recently identified (Adinolfi et al., 2003): NDF has been shown to interact with two nuclear partners of FMRP, the 82 KDa FMRP Interacting Protein (82-FIP) and the Nuclear FMRP Interacting Protein (NUFIP) (Bardoni and Mandel, 2002; Bardoni et al., 2003). Despite its importance, however, no structural information is available yet for this region of FMRP or for its mode of recognition of other proteins. In particular, a molecular insight into how FMRP selects specific protein partners in different phases of its functional cycle would be very important to rationalize the regulatory role of the protein.

We have used NMR spectroscopy to determine the structure in solution of NDF and to investigate its dynamic properties. This knowledge was used to identify key residues that are either involved in protein-protein interactions or determine the 3D arrangement of NDF. We prove that the structure as determined in our study reflects directly the in vivo 3D arrangement of the domain in full-length FMRP, since a double mutation designed to destabilize the NDF fold leads to a different cellular localization of FMRP and plays a role in subnuclear localization. The differences in the dynamic and functional properties of the NDF subdomains described hereby correlate the structural organization of NDF with its functional role.

Results

FMRP NDF Has Nonuniform Dynamic Properties

Despite the relatively small size of the domain, structure determination of NDF proved to be unexpectedly difficult, mostly because of its high tendency to be attacked by proteases and its dynamic properties: each NDF sample lasted no more than 5–7 days at room temperature after preparation, and the ^{15}N-^{1}H HSQC spectrum

*Correspondence: apastor@nimr.mrc.ac.uk

of NDF comprises a lower-than-expected number of crosspeaks with a distinct differential intensity (Figure 1A). Even under optimized salt conditions (10 mM NaCl), ~30 amide resonances are significantly broader than the rest. An additional increase of all of the resonance line widths was observed at higher salt (150 mM NaCl) or protein (>1 mM) concentrations, suggesting the occurrence of aggregation and/or conformational exchange phenomena. Little benefit could be obtained from varying the temperature far from 27ºC, as line width broadening was worse at low temperatures and higher temperatures promoted an even quicker degradation of the protein.

As a result, the spectral assignment of NDF proved unusually difficult and could be achieved only with the help of selectively and triple-labeled samples (for details, see Experimental Procedures). Despite this strategy, some of the backbone resonances could not be identified. After the backbone assignment was completed, the missing resonances were identified as being from loop residues, whereas the broad resonance amides were mostly mapped into the second half of the protein. In this region (around residues 90–111), both the TOCSY and NOESY transfer was poor, and some spin systems could be identified only tentatively, when detected at all. As a consequence, a larger number of restraints could be detected for the amino-terminal half of the domain (an average of 13.5 intradomain restraints were detected for residues 1–50, as compared to 9.5 for the region 63–113), as reflected from the higher precision of the resulting bundle of structures in this region (Figures 1B,C and Table 1).

Interestingly, no intermolecular NOEs could be identified in normal NOESY-HSQC experiments or in a ^{13}C half-filtered 2D NOESY (Otting and Wuethrich, 1989) recorded with an NDF sample obtained by mixing independently produced batches of ^{12}C- and ^{13}C-labeled protein. This is in contrast to the presence of the stable, dimeric form expected on the basis of previous ultracentrifugation experiments (Adinolfi et al., 2003). A stable dimer is also hardly compatible with the high protease susceptibility and with the apparent intrinsic flexibility of the domain (see also the relaxation parameters discussed below). Possible, not mutually exclusive, explanations are that dimerization is part of a process of unspecific aggregation caused by the absence of other regions of the protein that could stabilize the dimer, and/or that the dimerization interface involves only a limited surface. We are currently exploring these possibilities. Meanwhile, the structure of the monomer constitutes the best structural model available to investigate the molecular interactions formed by NDF.

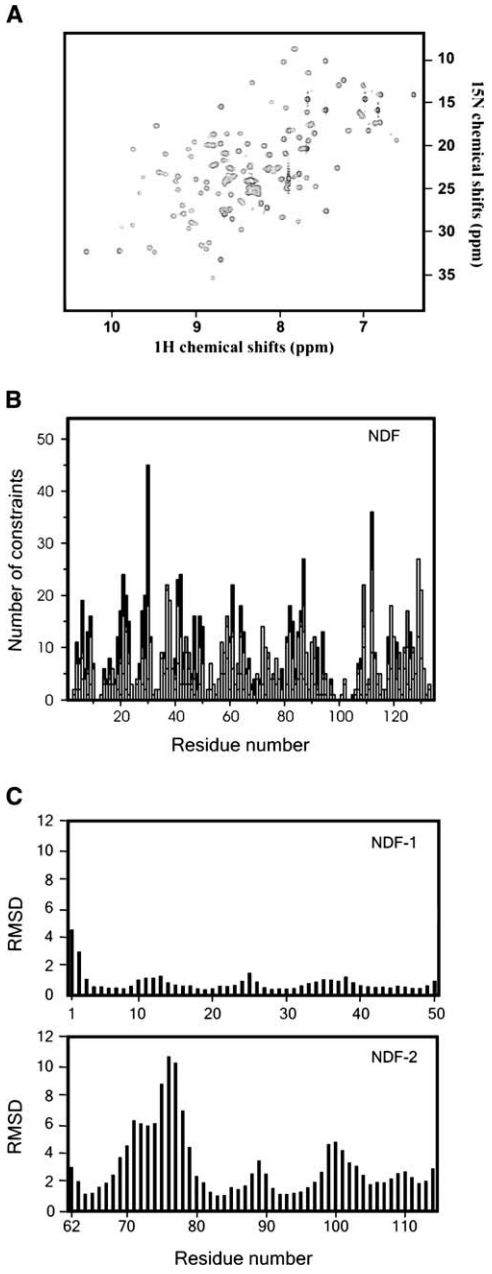

Figure 1. NMR Spectrum of NDF and Indicators of the Restraint Distribution and of the Structure Precision along the Sequence

(A) ^{15}N-^{1}H HSQC spectrum of NDF recorded at 27ºC and 600 MHz on a 0.6 mM protein solution in 10 mM Tris-HCl (pH 7.4), 10 mM NaCl, and 2 mM β-mercaptoethanol.

(B) Number of NOE restraints plotted versus the NDF sequence. Region 95–105 is relatively more poorly defined.

(C) Rmsd of the structure bundle versus the sequence. The two repeats are plotted separately to facilitate comparison.

FMRP NDF Has a Complex Subdomain Organization

The solution structure of the NDF monomer consists of two repeats, which we named NDF-1 (spanning residues 3–50 of FMRP) and NDF-2 (spanning residues 63–113), joined by an unstructured linker and followed by a tail of 20 amino acids (Figure 2). Each repeat folds into a bent four-stranded antiparallel β sheet, with a fifth strand closing the cavity of the sheet, similar to a thumb across a semiclosed hand. Although NDF-1 and -2 have qualitatively very similar features, NDF-2 is less compact (300 $Å^2$ extra exposed surface) well-defined, with a root mean square deviation (rmsd) for the backbone atoms of 1.66 Å, as compared to 0.74 Å calculated for NDF-1. The relative orientation of the two NDF subdomains cannot be precisely determined (Figure 2), and the overall backbone rmsd is 2.98 Å. Some important features are nevertheless common to all of the structures of the bundle. First, the axis joining the β sheets of the two repeats runs approximately parallel to the longitudinal axis of NDF, and the two repeats are rotated by ~90º

Table 1. Structural Statistics for the NDF Domain of FMRP

Final NMR restraints			
Total distance restraints	1466		
Intraresidue	728		
Sequential	408		
Medium (I to I + j, 2 = j = 4)	115		
Long (I to I + j, j = 4)	215		
H bonds	34		
ψ and ϕ	146		
Restraint violations[a]			
Distance restraint violations > 0.5 Å	0.5		
Angle restraint violations > 5°	1.25		
	NDF-1	NDF-2	All
Coordinate precision[b]			
All residues	0.74/1.37	1.66/2.27	2.98/3.42
Secondary structure	0.38/1.05	0.56/1.36	2.06/2.54
WHATIF quality check			
Packing	−1.05	−3.73	−4.43
Ramachandran	−1.18	−2.92	−3.33
$\chi1/\chi2$	−2.98	−4.39	−2.90
Backbone conformation	−2.40	−3.47	−4.27
Procheck Ramachandran statistics			
Most favorable	80.7%	71.0%	72.4%
Additionally allowed	14.2%	18.0%	17.8%
Generously allowed	3.7%	6.0%	5.5%
Disallowed	1.4%	5.0%	4.3%

[a] Average per structure of the bundle.
[b] Rmsd in Å to mean structure. Backbone/heavy atoms.

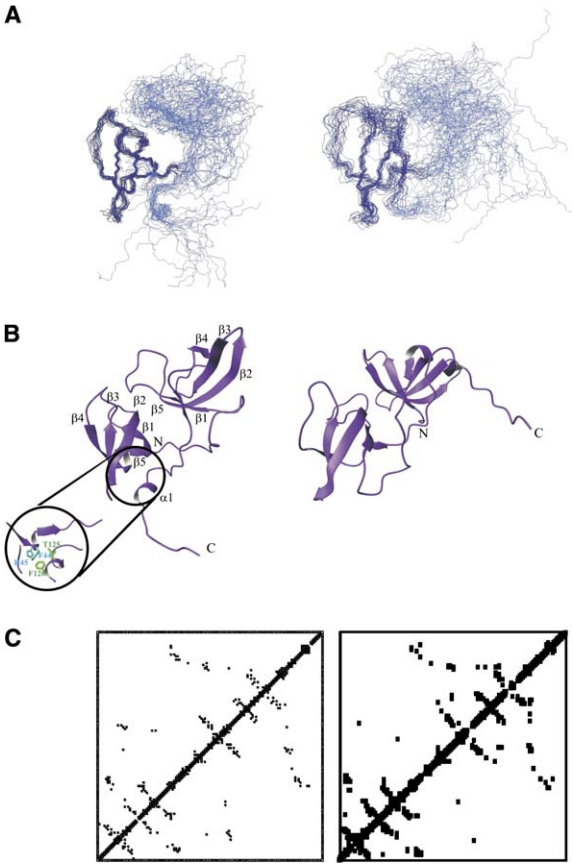

Figure 2. The Structure of NDF and the Interactions between Its Subdomains

(A) NMR bundles of the best 20 XPLOR structures. The NDF-1 and NDF-2 repeats were superposed separately, colored in dark blue. The relative orientation of the two repeats is underdefined, shown by displaying each repeat alternatively in the same orientation.

(B) Ribbon representation of the best energy structure. The orientation is the same as that shown for (A). The secondary structure elements and the N and C termini of the construct are labeled. Inset: Details of the packing of $\alpha1$ against NDF-1.

(C) Comparison between the experimental map of interresidue NOEs (right) and the distance map as calculated from the energetically best NDF structure (left). The distance map was generated by the WHATIF program (Vriend, 1990). A cutoff of 2.5 Å was added to the van der Waals radii.

from each other. Second, direct contacts between the two repeats are formed between the $\beta1$-$\beta2$ and $\beta3$-$\beta4$ loops of NDF-1, with the $\beta3$-$\beta4$ and $\beta1$-$\beta2$ loops of NDF-2, respectively, burying a surface of 453 Å^2. A key role in these interactions is played by aromatic residues (Phe15, Trp79, Trp80). The linker and the first six amino acids of the C-terminal tail are sandwiched between the two repeats (Figures 2B and 2C). Finally, the C-terminal tail (amino acids 114–134) is unstructured, with the exception of amino acids 122–126, which fold into a one-turn helix ($\alpha1$) and whose side chains pack against NDF-1, forming a small hydrophobic core. This interaction buries a relatively extended patch of ~360 Å^2 and confers a more globular shape to the entire domain.

Relaxation Analysis Allows Us to Study the Dynamics of NDF

To investigate the dynamic behavior of NDF, ^{15}N T_1, T_2 and ^{15}N $\{^1H\}$ NOE experiments were recorded (Figure 3). Analysis of NDF ^{15}N $\{^1H\}$ NOE and T_1 values indicates that the two repeats are more rigid than the other elements. NDF-2 is more flexible than NDF-1, with an increase of flexibility most noticeable in loop regions. The C-terminal tail and the NDF-1/NDF-2 linker are overall very flexible, as shown by the heteronuclear NOE values, with the exception of residues Thr125 and Phe126 in $\alpha1$, whose side chains pack against NDF-1. This suggests that $\alpha1$ is a stable structural element. Higher than average ^{15}N T_1/T_2 ratios and short T_2 values were observed for the residues of the $\beta3$-$\beta4$ loop of NDF-1, which contacts NDF-2, and for ten NDF-2 residues, several of which are located in secondary structure elements. This indicates that these two regions undergo motions in the millisecond timescale. This dynamic behavior is often associated with the presence of a conformational exchange on a biologically relevant timescale.

Analysis of the T_1/T_2 ratios in structured protein regions reveals that the NDF has a correlation time (τ_c) of approximately 14 ns. This value is larger than the one expected for a 15.5 kDa protein monomer and is between that expected for a monomer and a dimer (Maciejewski et al., 2000). This is consistent with what is discussed above.

The NDF-1 and NDF-2 Repeats Belong to the "Royal" Domain Superfamily

A recent comparative study by Mauhrer-Stroh and coworkers based on sequence analysis identified a new family, named Agenet, of mainly plant protein domains

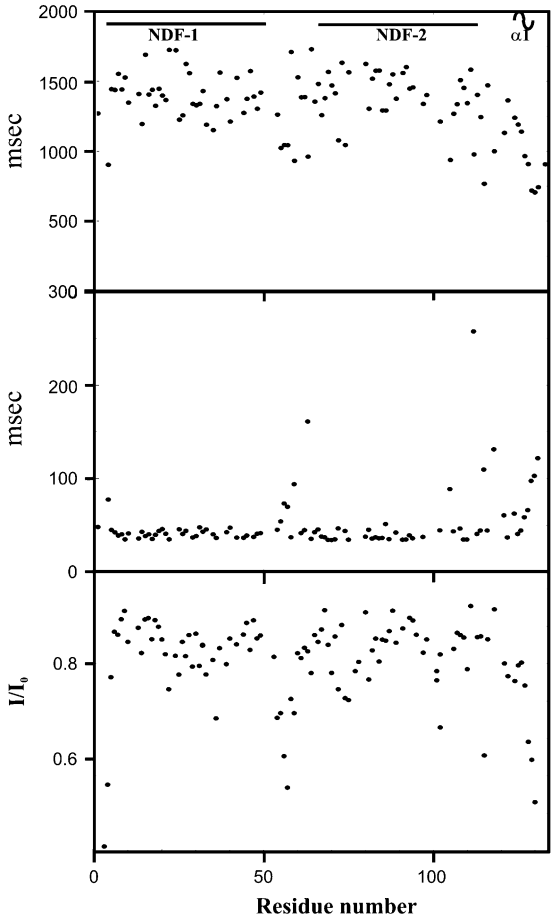

Figure 3. Relaxation Data of NDF

Top to bottom, plots of backbone amides ^{15}N T_1, T_2, and ^{15}N $\{^1H\}$ NOE values versus the NDF sequence. The data were collected at 27°C and 800 MHz. The positions of NDF-1, NDF-2, and α1 are indicated. The values of ^{15}N T_1, T_2, and ^{15}N $\{^1H\}$ NOE can be found in Table S1 (see the Supplemental Data available with this article online).

(Maurer-Stroh et al., 2003). Agenet domains were suggested to share a four β strand fold with chromo, MBT, and Tudor domains and to be part of a "Royal" domain superfamily. In the same study, the N terminus of FMRP was proposed to contain two repeats of the Tudor/Agenet motif.

Accordingly, we observe two repeats in NDF, and, when the coordinates of NDF-1 and NDF-2 were independently submitted to the EBI Dali server, significant matches were obtained almost exclusively with proteins of the "Royal" family. The closest match to the better-defined NDF-1 is the Tudor domain of the SMN protein (Selenko et al., 2001) (1g5v). The two structures superpose on 47 residues over a total of 48 with a 1.9 Å rmsd, despite the two domains sharing a fairly low sequence identity (15%). Superposition of the two domains (Figure 4A) clearly shows that all five β strands of NDF-1 align with the corresponding β strands of SMN, thus suggesting redefinition of the boundaries of the Tudor/Agenet domains to include an extra β strand (Figure 4B). The two next highest matches select the DNA binding domain of HIV-1 integrase (Lodi et al., 1995) (1ihv) and the transcription elongation factor NusG from *Thermus thermophilus* (Reay et al., 2004) (1nz9), which superpose with 2.0 Å and 2.4 Å over 45 and 48 residues, respectively (Figure 4A).

NDF Interacts with Trimethylated Lysine through a Hydrophobic Cavity of NDF-2

The structural similarity between other Tudor domains (Figure 4A) and the NDF repeats suggests that they may at least partially recognize structurally similar targets, such as symmetrically methylated arginine and lysine residues. To investigate this hypothesis, ^{15}N-labeled NDF was titrated with symmetrically methylated arginine, asymmetrically methylated arginine, nonmethylated arginine, methylated lysine, and nonmethylated lysine up to a 1:25 molar ratio. A similar test was successfully used in a study of the binding specificity of the SMN Tudor domain and provided evidence for the role of methylation in the recognition of the SMN hydrophobic cavity by its targets (Sprangers et al., 2003). Chemical shift variations of the protein resonances were followed by recording ^{15}N-^1H HSQC experiments at each titration point. Nonmethylated amino acids and methylated arginine did not cause significant chemical shift variations (data not shown), whereas methylated lysine caused small, but appreciable, shifts of selected resonances (Figure 5A). When these variations are mapped onto the NDF structure, they all correspond to residues that cluster in the loops flanking a hydrophobic cavity of NDF-2 and involve roughly the same surface found to interact with methylated residues in the SMN Tudor and HP1 chromo domains (Sprangers et al., 2003; Nielsen et al., 2002) (Figure 5B). NDF-1 resonances were not affected. Although both NDF repeats have similar hydrophobic cavaties, that of NDF-1 is protected by the C-terminal tail and by the β1-β2 loop of NDF-2.

These results suggest a selective and specific role of NDF-2 in the recognition of methylated lysine targets.

NDF-2 Mediates the Interaction with 82-FIP

A representation of the hydrophobic surface of NDF reveals other exposed hydrophobic patches in addition to those responsible for interaction with methylated lysine, which could, in principle, be available for molecular interactions with other partners (Figure 6A). To investigate the interaction between FMRP and 82-FIP, we subcloned and expressed a peptide corresponding to amino acids 255–411 of 82-FIP (82-FIP156), which spans the region found to be necessary for binding (Bardoni et al., 2003). ^1H 1D and ^{15}N-^1H HSQC NMR spectra of 82-FIP156 showed that this peptide is largely unfolded (data not shown). Titration of ^{15}N-labeled NDF with unlabeled 82-FIP156 to reach a 1:2 final molar ratio resulted in the broadening and disappearance of all amide resonances of NDF-2 and most of the ones at the NDF-1/NDF-2 interface, while the majority of NDF-1 resonances and those of the NDF-1/NDF-2 linker and of the C-terminal tail were still clearly detectable (Figure 6B,C). This result was further confirmed by analysis of the aromatic and aliphatic resonances in ^{13}C-^1H NDF spectra. For comparison, titration of NDF with other largely unfolded domains of FMRP (e.g., FMRP KH2 domain and a peptide encompassing the RGG box) did not result in any appreciable spectral variation (data not shown).

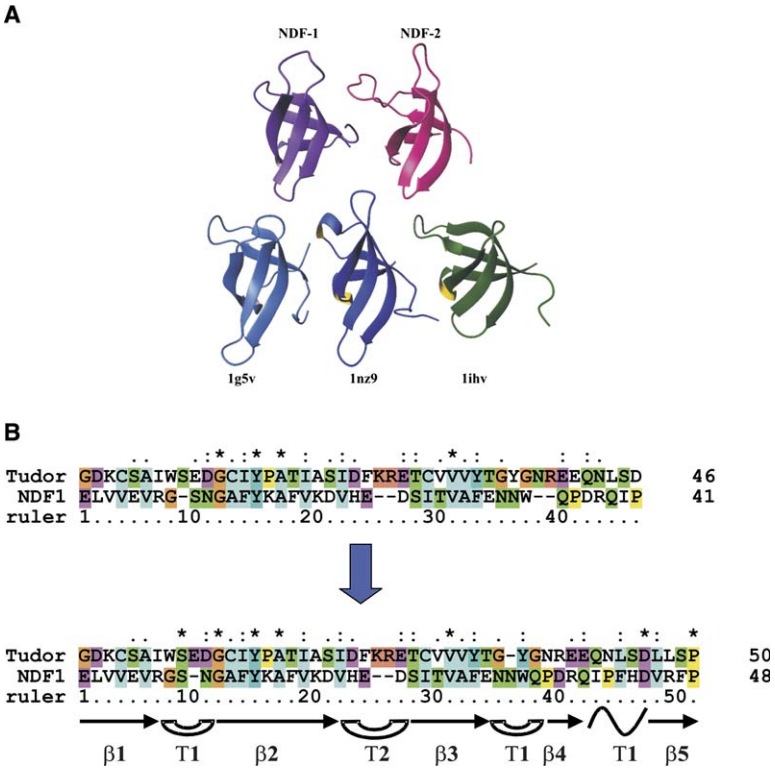

Figure 4. Comparison between the Two NDF Repeats and Other Tudor Domains

(A) Structure comparison of NDF-1 and NDF-2 and the three highest hits of a structure database search. NDF-1 and NDF-2 are shown in purple and pink, respectively. The Tudor domain of the SMN protein (1g5v), the DNA binding domain of HIV-1 integrase (1ihv), and the transcription elongation factor NusG from *Thermus thermophilus* (1nz9) are shown in light blue, dark blue, and green, respectively. The structures were all superposed pairwise on that of NDF-1 and then translated.

(B) Comparison between the published alignment of Tudor/Agenet domains and that obtained by using the structural information described in this paper. The secondary structure elements as observed in the NDF-1 structure are indicated under the alignment.

The Tandem Arrangement of Three Structural Motifs Is Essential for NDF Stability

The structure of NDF shows that this domain is constituted by three structural motifs, i.e., the two NDF repeats and α1. Extensive interactions are observed between these elements (see above), thus strongly suggesting that their copresence is necessary for the stability of the overall domain. To test this hypothesis, we tried to express the two NDF repeats without the addition of the tail containing α1. When a C-terminally shorter version of NDF (amino acids 1–120) was produced, the construct expressed with a very poor yield (by far insufficient for any structural characterization) and was highly prone to aggregation. Another interesting, albeit indirect, indication was obtained by observing that degradation of NDF at 27ºC is slow and, initially, does not affect drastically the fold of the protein. However, after ca. 1 week, the protein unfolds rapidly. Gel and mass spectrometry analyses showed that degradation initiates by cleavage of a C-terminal fragment that spans residues 122–134. Given these indications, we did not attempt to produce the isolated NDF-1 or NDF-2.

We designed instead a double mutant in which T125 and F126, the two residues involved in the interaction between NDF-1 and α1, were mutated to alanines (T125A/F126A double mutant). This choice should prevent the formation of the two key hydrophobic interactions essential for packing α1 against the NDF-1 hydrophobic cavity while preserving the secondary structure of α1. Without this interaction, we expected a strong destabilization of the 3D arrangement of NDF. Accordingly, when the NDF T125A/F126A double mutant was produced in *E. coli* as a GST fusion protein, most of the protein went into inclusion bodies (data not shown). The supernatant was nonetheless processed further, and an affinity column (Ni-NTA gel) was used to purify the fusion protein. A detectable amount of protein was present in the eluted fractions from the affinity column but immediately precipitated, as confirmed by standard colorimetric assays performed on the soluble portion after centrifugation.

These results confirm that all three structural motifs are essential for the stability of the NDF fold.

Destabilization of the NDF Fold Causes a Different Cellular Localization of FMRP

To understand how destabilization of the NDF fold, as observed in the T125A/F126A double mutant, could affect the functions of FMRP, we set up a functional assay in which full-length FMRP localization was tested in a eukaryotic cell model. This assay was developed because the N terminus of FMRP is known to be involved in cellular compartmentalization of the protein (Bardoni and Mandel, 2002). Both the well-characterized FMRP isoforms 7 and 12 (ISO7 and ISO12) were used. ISO7, the most abundant isoform in adult tissues, is known to localize in the cytoplasm, whereas ISO12 lacks the nuclear export signal (NES) and thus localizes prevalently in the nucleus, mostly in the perinucleolar region (Bardoni and Mandel, 2002; Willemsen et al., 1996; Khandjian, 1999). For each isoform, in vitro-prepared COS cells were transfected for 12 hr with two different clones of the double mutant and of the wild-type, in separate experiments. After cell fixation, immunofluorescence was performed by using the 1C3 antibody, which recognizes the amino-terminal region of FMRP (Devys et al., 1993). For ISO7, no differences in localization of the two proteins were observed: both localize in the cytoplasm. Conversely, while wild-type ISO12 localizes in the nucleus and in particular around the nucleoli, as previously

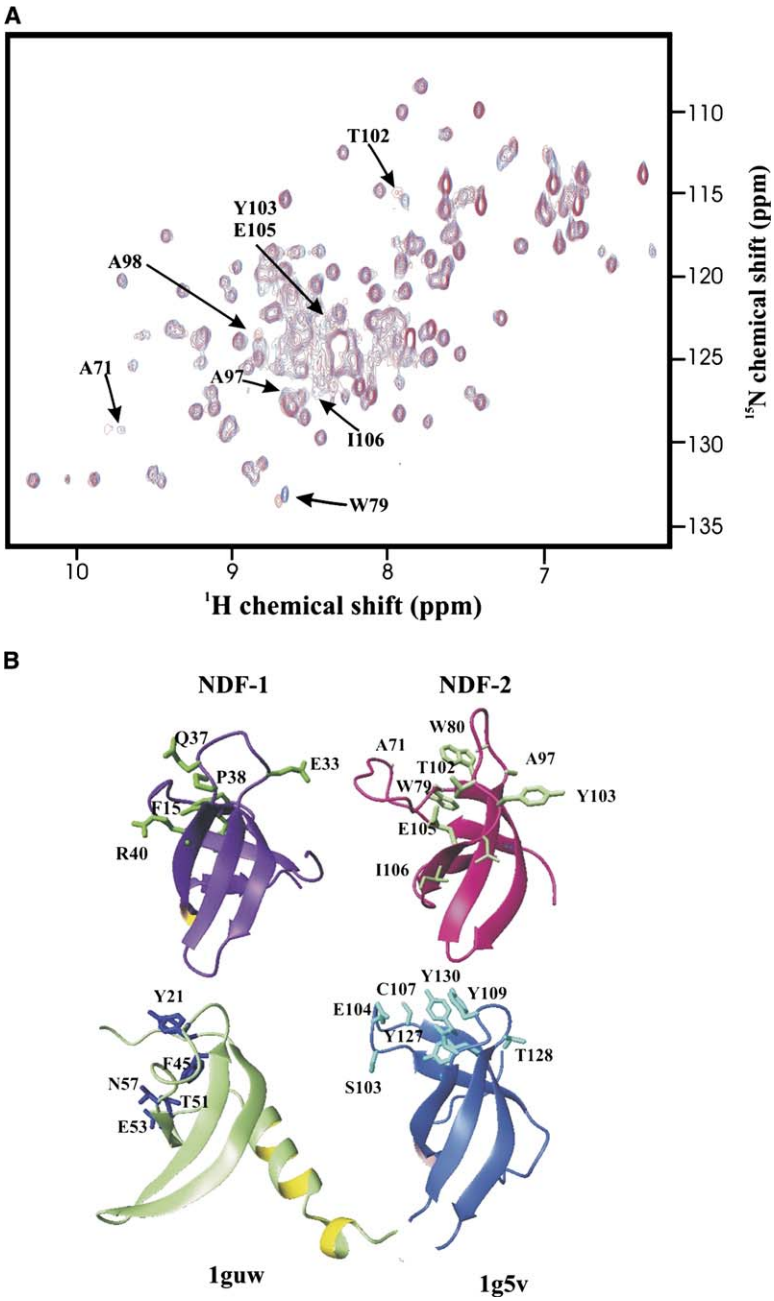

Figure 5. Interaction of NDF with Trimethylated Lysine

(A) Superposition of the HSQC spectra of NDF in the absence (red) and in the presence (blue) of methylated lysine (1:25 protein: amino acid ratio). The crosspeak of Trp80 at 9.90 ppm and 129.9 ppm is too weak to be visible with the selected threshold.

(B) Mapping of the residues involved in the interaction with methylated lysine on the NDF-2 surface. For comparison, the corresponding residues of NDF-1 and those reported to bind the Tudor domain of the SMN protein (1g5v) and of HP1 chromodomain (1guw) are reported. The structures have the same orientation as in the left panel of Figure 2B.

reported (Bardoni and Mandel, 2002) (Figure 7), the perinucleolar localization of the double mutant is almost completely lost. Although still mainly localized in the nucleus, the ISO12 double mutant localizes around the nucleoli only in 2% and 6% of the cells as compared to 63% for wild-type ISO12. This indicates that the fold of the isolated NDF as we observed in solution reflects that of the full-length protein and that the domain is involved in nucleolar localization of FMRP.

Discussion

FMRP is a modular protein thought to be involved in different cellular functions, as supported by the several molecular partners identified so far (Bardoni et al., 1999; Jin and Warren, 2003). Since many of these interactions map to sequence-adjacent or overlapping regions of the protein, a deeper understanding of how they might be modulated is a prerequisite for dissecting the regulatory mechanism of FMRP. One of the regions known to be involved in several different protein-protein interactions is NDF, which spans the first 134 N-terminal amino acids of FMRP (Adinolfi et al., 2003). We have shown here, through the structure determination of this domain, that the isolated NDF is a relatively noncompact domain, in line with the hypothesis that, in the full-length protein, the N terminus of FMRP is stabilized by interactions with other regions of the molecule and/or with other molecular partners (Adinolfi et al., 2003). NDF comprises three structural motifs, the two NDF-1 and -2 repeats, and the C-terminal helix. Despite a relatively low sequence identity, NDF-1 and NDF-2 share a significant

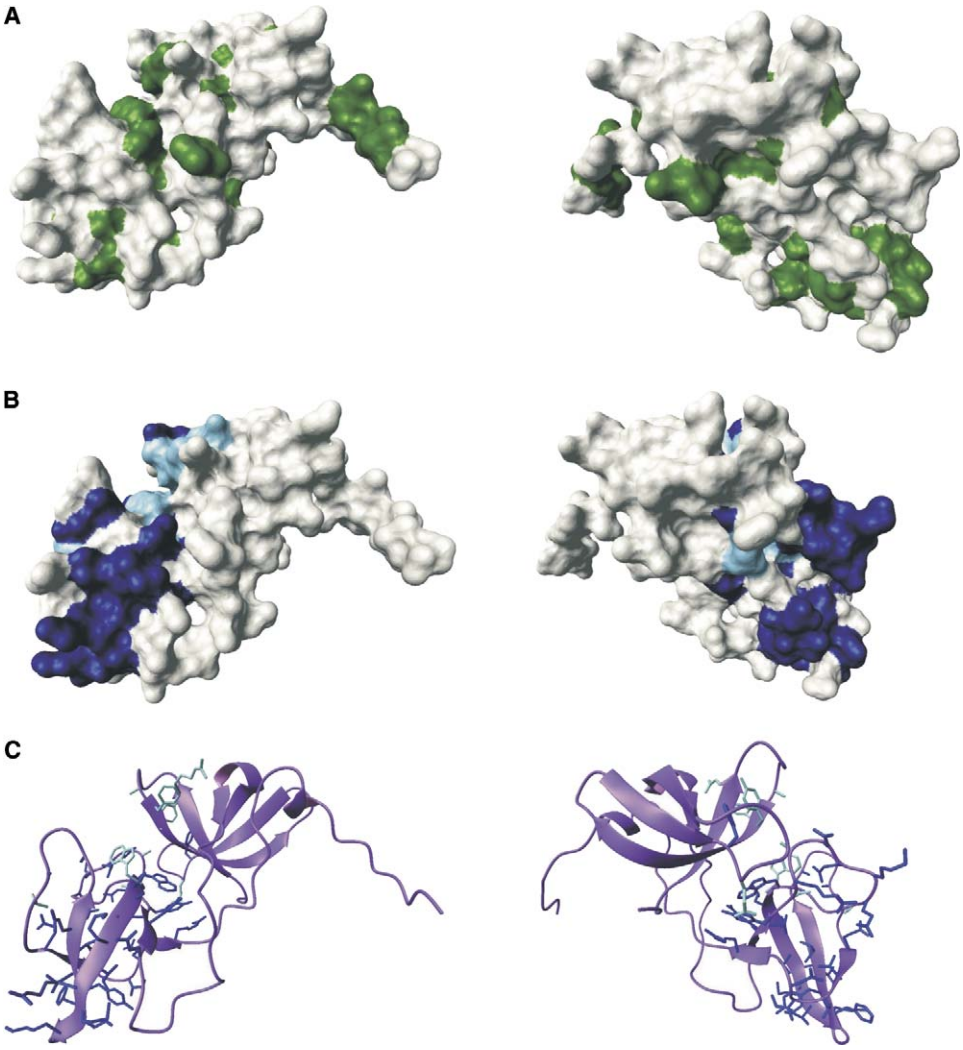

Figure 6. Mapping the Interaction Surface of 82-FIP onto the NDF Structure

(A) Exposed hydrophobic patches (green) are shown on two surface representations of the NDF structure (white) that differ by a 180° rotation around the y axis. The orientation of the NDF structure on the left is the same as that in the right panel of Figure 2B.

(B) Residues involved in the interaction with 82-FIP156. The side chains of the residues that lead to marked (10, 13, 32, 64, 66, 67, 68, 70, 72–75, 79, 81–89, 91–95, 98, 101, 105, 107–110, 113) and minor (9, 14–16, 33, 69, 71, 80, 102) variations of the peak intensities in the HSQC are displayed in dark blue and light blue, respectively.

(C) Same as in (B), but in a ribbon representation showing explicitly the side chains of the residues affected.

structural similarity with the SMN Tudor domain, in agreement with fold predictions (Reay et al., 2004). Using the structural information obtained from our study, we propose to redefine the domain boundaries of the Tudor/Agenet domain family and suggest a consensus sequence that could be used for identification of new members of the "Royal" domain superfamily.

The NDF structure reveals hydrophobic pockets on the surface of the two repeats, which, in analogy with other Tudor domains, such as the SMN Tudor and the HP1 chromo domains (Sprangers et al., 2003, Nielsen et al., 2002), are likely to be involved in protein-protein interactions. Indeed, our studies show that one of the NDF hydrophobic pockets binds to methylated amino acids with a clear target specificity: we observed no binding between NDF and dimethylated arginine, the residue suggested to be the preferential substrate of SMN, but we observed specific recognition of methylated lysine, the target of HP1 (Sprangers et al., 2003, Nielsen et al., 2002). This indicates that methylation may play a regulatory role in the interaction of FMRP with a functional partner, as is the case for other proteins containing domains of the "Royal" superfamily. Interestingly, only NDF-2 is involved in the interaction with the methylated amino acid. Binding to the nuclear 82-FIP protein is also mainly mediated by the flexible NDF-2. This is in agreement with an earlier report that showed that substitution of the amino acid 66–134 region of FMRP with the equivalent region of the closely related FXR1P is sufficient to abolish interaction with 82-FIP and NUFIP (Bardoni et al., 2003). Binding of both 82-FIP and methylated lysine to the more open and flexible NDF-2 suggests that the two NDF repeats, although structurally similar, have very different functional and dynamic properties.

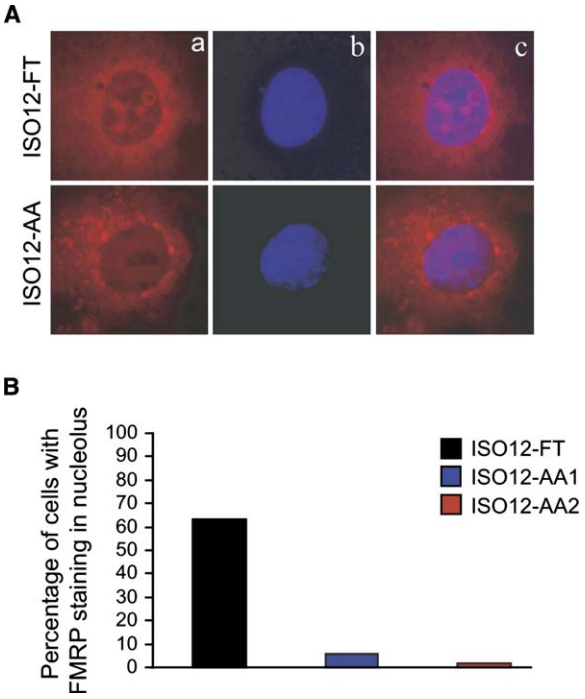

Figure 7. Loss of Nucleolar Localization of the ISO12 Double Mutant in COS Cells

(A) COS cells were transfected with the wild-type FMRP ISO12 (ISO12-FT), or with two independent clones of double mutant T125A/F126A ISO12 (ISO12-AA1 and ISO12-AA2). ISO12 is labeled in red (column a). Nuclei are stained with Hoechst dye (column b). The two images were then merged (column c).

(B) Percentage of cells exhibiting FMRP ISO12 perinucleolar staining (wild-type and mutants). More than 85 transfected COS cells were analyzed for each assay.

Therefore, NDF-2 seems to be a stronger target for interactions, possibly because of its plasticity and availability of exposed hydrophobic cavities.

Finally, we have shown that mutation of two residues of α1, T125 and F126, which are crucial for the interaction with NDF-1 and therefore for determining the stability of the NDF fold, results in loss of FMRP localization in the perinucleolar region of COS cells, whereas it has no effect on cytoplasmic or nuclear localization. A similar alteration of nucleolar localization by using suitable deletion mutants has been described for other proteins, such as the Tudor-containing SMN (Lefebvre et al., 2002) and nucleolin (Schmidt-Zachmann and Nigg, 1993). Perinucleolar localization of a protein can be achieved either by a nucleolar localization signal or by interaction with other proteins containing this signal. An example of this second mechanism is provided by nucleolin, which "piggy-backs" on nucleolar localization factors to reach its RNA targets (Schmidt-Zachmann and Nigg, 1993). FMRP, which does not contain a known nucleolar localization sequence motif, could function in a similar way.

The NDF structure, with its complex modular fold formed by three distinct structural motifs, suggests how nucleolar localization and other functions could be mediated by this domain. Several single Tudor motifs are able to fold as independently folded units (domains) when separated from the protein context. The two Tudor domains of NDF are instead rather flexible, and the presence of α1 seems to be necessary to achieve a relatively compact domain with a relatively modest thermal stability (52ºC) (Adinolfi et al., 2003). We may therefore speculate that the complexity of the NDF 3D arrangement may constitute the basis of an "allosteric" regulatory mechanism able to fine tune the selection of the different protein partners of FMRP during the different phases of its functional cycle. Under this hypothesis, the plasticity and modularity of the three subdomain fold of NDF could provide a simpler and more flexible mechanism than that obtainable by a compact single domain: the possibility of reorienting and stabilizing one or more of the NDF subdomains would allow modulation of the interactions with other cellular partners, directly or by mediation of other regions of FMRP. The example of NDF may constitute a paradigm that is also valid for other translational regulatory proteins that form different interactions at different functional stages.

In conclusion, the work presented above illustrates how a relatively short region of FMRP may have a complex subdomain organization able to fulfill a range of diversified functions. It also provides the structural framework for the design of new experiments aimed at a better understanding of the relationship between FMRP and its ever-increasing group of cellular partners, as these are gradually identified.

Experimental Procedures

Protein Preparation

The NDF construct, which spans amino acids 1–134 of FMRP, preceded by two residues added for cloning and purification purposes, was overexpressed as a histidine-tagged GST fusion protein in *E. coli* BL21 DE3 and was purified by using a two-step protocol. After breaking the cells in the recommended buffer (Pharmacia), the soluble fraction was loaded onto a Ni^{2+} semiaffinity column, and the matrix was extensively washed. The protein was eluted in 300 mM imidazole, dialyzed against 10 mM imidazole buffer, and cleaved from GST by overnight Tobacco Etch Virus (TEV) protease digestion at 25ºC. The digestion product was loaded on a fresh nickel-affinity column to remove the histidine-tagged TEV protease and GST. The NDF flowthrough was concentrated and dialyzed against the final buffer. ^{15}N-labeled and ^{15}N-^{13}C-labeled proteins were obtained by expressing GST-NDF in M9 minimal media supplemented with ^{15}N ammonium sulfate and, for the doubly labeled protein, ^{13}C glucose as the sole nitrogen and carbon sources, respectively. ^{2}H, ^{15}N, and ^{13}C triply labeled NDF were also obtained by growing the bacteria in $^{2}H_2O$ minimal media. The homogeneity and molecular weight of unlabeled NDF were confirmed by electrospray mass spectrometry.

An unlabeled shorter version of NDF (amino acids 1–120), a construct spanning amino acids 255–411 of human 82-FIP (Bardoni et al., 2003) (82-FIP156) and the T125A/F126A double mutant were subcloned into the same GST fusion vector from the original clones and expressed and purified by following the same strategy as described above.

NMR Spectroscopy Studies

NMR spectra were recorded at 27ºC on Varian INOVA and UnityPlus spectrometers operating at 500, 600, and 800 MHz ^{1}H frequencies and on a Bruker Advance spectrometer operating at 600 MHz ^{1}H frequency equipped with a cryoprobe. The experiments were recorded with 0.6 mM samples of NDF in a 90% H_2O/10% D_2O mixture in 10 mM Tris-HCl (pH 7.4), 10 mM NaCl, and 2 mM β-mercaptoethanol. Preliminary experiments to screen the experimental conditions were also carried out in the same buffer as described above, but with 150 mM NaCl. Water suppression was achieved by WATERGATE pulse sequences (Piotto et al., 1992). The spectra were processed

and zero filled to the next power of two by using the NMRPIPE program (Delaglio et al., 1995). Baseline correction was applied when necessary. Spectral analysis was performed by using Felix (Accelerys) and XEASY (Bartels et al., 1995).

Because of the dynamic properties of the construct, the assignment had to be assisted by specifically designed strategies. Sequential assignment was obtained by using a combination of TROSY-like experiments, triple-labeled, and selectively labeled samples. TROSY versions of HNCO, HNCA, and HNCACB experiments recorded on ^{2}H, ^{15}N, and ^{13}C triply labeled samples proved essential for backbone assignment. The assignment was then confirmed by leucine and valine individually ^{15}N-selectively labeled samples. Side chain assignment was mostly achieved by using data from ^{13}C-edited NOESY spectra, as through-bond correlation experiments failed to give satisfactory results. Aromatic optimized HCCH-TOCSY and ^{13}C-edited NOESY experiments were the basis for aromatic proton assignment, while the success of (Hβ)Cβ(CγCδ)Hδ and (Hβ)Cβ(CγCδ Cε)Hε experiments was limited. Even with the ad hoc strategy adopted, some resonances were missing at the end or could only be assigned tentatively. They included the amides of S11, N12, N34, E90, Y96, C99, and Y103 and some of the side chain protons of Y96, C99, D100, Y103, and E105. Most of the uncertainties cluster in the C terminus of NDF2. In total, ~87% of nitrogen, amide, Hα, Cα, and CO resonances and ~75% of side chain resonances were finally assigned.

Structure Calculation

Distance restraints were extracted from a ^{15}N-edited 3D NOESY (150 ms mixing time) and two ^{13}C-edited 3D NOESY experiments (one with carrier and spectral width optimized for aromatic resonances) with 100 ms mixing times. An HNHA experiment (Vuister and Bax, 1993) was recorded to obtain semiquantitative information on H^{N}-H^{α} J couplings.

Amide proton protection was obtained by recording a series of 80 ^{15}N-^{1}H HSQC experiments (each with a 30 min acquisition time) on a ^{15}N-labeled sample of NDF freeze dried and redissolved in a 100% D_2O solution. A ^{13}C half-filtered 2D NOESY experiment (Otting and Wuethrich, 1989) was recorded to detect a possible dimerization surface, on a 0.5 mM sample of FMRP obtained by mixing two samples of ^{12}C and ^{13}C protein. The experiment was repeated after freeze drying the protein and resuspending it in a 100% D_2O solution to eliminate unwanted amide proton resonances.

Automatic calculation of NOE crosspeak volumes was initially attempted by using SPSCAN (http://www.molebio.uni-jena.de/~rwg/spscan) and the XEASY integration routine (Bartels et al., 1995). Peak volumes were then converted into interproton upper limit distance restraints by the program CALIBA (Guntert et al., 1997). However, the strong variability of the resonance line widths and intensities and the relatively low signal-to-noise ratio experienced for some peaks led to an inconsistent set of distance restraints, as judged from equivalent distances measured on known secondary structures. We therefore adopted a semiautomated procedure, in which the peak intensities were obtained by XEASY and the restraints were manually calibrated by assuming known distances in secondary structure elements. A fixed correction was applied for peak overlap or very broad peaks. Angular restraints (ϕ and ψ) were obtained from chemical shift values of N, Hα, Cα, Cβ, and CO resonances by using TALOS (Cornilescu et al., 1999). Hydrogen bond restraints were introduced only after the initial calculation phase. They were imposed only if the corresponding proton was observed as protected in hydrogen exchange experiments and if, in the preliminary calculations, the same hydrogen bond was formed in all of the 20 best structures.

Structure calculations were first performed by the program CYANA (Guntert et al., 1997), by using a standard torsion angle dynamics protocol and upper-distance, angular, and hydrogen bond restraints. The structures were then refined by using restrained molecular dynamics within the XPLOR program (Schwieters et al., 2003) and a CHARMM22 water refinement protocol (Spronk et al., 2002). The quality of the obtained set of structures was evaluated by the PROCHECK (Laskowski et al., 1996) and WHATIF programs (Vriend, 1990).

Relaxation Studies

^{15}N T_1 and T_2 experiments were recorded at 800 MHz proton frequency on a ^{15}N-labeled 0.8 mM NDF sample by using standard sequences (Kay et al., 1992). Peak intensities as a function of delay time were extracted from the spectra and normalized to the intensity of the first data point by using the NMRPIPE/NMRDRAW package. The T_1 and T_2 values were determined by least-square fitting to a single exponential decay for each peak. Experimental errors (signal-to-noise) are reported in the Supplemental Data available with this article online. ^{15}N $\{^{1}H\}$ NOE values were obtained by recording interleaved ^{15}N-^{1}H correlated experiments for a total acquisition time of 48 hr and calculating the peak intensity ratios as extracted from experiments with and without presaturation. Indicative correlation times were calculated from an average T_1:T_2 ratio in secondary structure elements by using the model-free approach (Lipari and Szabo, 1982).

NMR Binding Assays

82-FIP binding to NDF was tested by titrating unlabeled 82-FIP156 into a 0.3 mM sample of ^{15}N-labeled NDF dissolved in 10 mM Tris-HCl (pH 8), 10 mM NaCl, and 2 mM β-mercaptoethanol up to a 2:1 molar ratio and recording ^{15}N-^{1}H HSQC TROSY-type experiments at each step of the titration. The titration was repeated on a ^{13}C-labeled NDF sample recording ^{13}C-^{1}H HSQC experiments, optimized both for aromatic and aliphatic protons. Binding of methylated and nonmethylated arginine and lysine to NDF was tested by adding a concentrated solution of the amino acid to a 0.3 mM sample of ^{15}N-labeled NDF in 10 mM Tris-HCl (pH 7.7), 10 mM NaCl, and β-mercaptoethanol up to a 25:1 amino acid:protein molar ratio.

In vivo mutagenesis

T125 and F126 of the FMRP ISO12 isoform were mutated into alanines and cloned in the pTL1 vector (Sittler et al., 1996). The mutagenesis was performed by using the QuickChange Site-Directed Mutagenesis Kit (Stratagene) according to the manufacturer's instructions and oligos 5′-CCTGCCACAAAAGATGCTGCCCATAAGA TCAAGCTGGATGTGC-3′ and 5′-GCACATCCAGCTTGATCTTATGG GCAGCATCTTTTGTGGCAGG-3′.

Immunofluorescence and Western Blots

Cells were transfected for 12 hr by using Effectene TM (Qiagene). Immunofluorescence and Western blots were performed as previously described (Sittler et al., 1996). FMRP was detected by using the monoclonal anti-FMRP antibody 1C3[32] as previously described (Sittler et al., 1996).

Supplemental Data

Supplemental Data including a table of NMR relaxation parameters are available at http://www.structure.org/cgi/content/full/14/1/21/DC1/.

Acknowledgments

The work was supported by a Human Frontiers Science Program grant. B.B. also acknowledges financial support from CNRS and from the French Fondation pour la Recherche Médical.

Received: May 7, 2005
Revised: September 6, 2005
Accepted: September 9, 2005
Published: January 10, 2006

References

Adinolfi, S., Ramos, A., Martin, S.R., Dal Piaz, F., Pucci, P., Bardoni, B., Mandel, J.L., and Pastore, A. (2003). The N-terminus of the Fragile X Mental Retardation Protein contains a novel domain involved in dimerisation and RNA-binding. Biochemistry *43*, 10437–10444.

Bardoni, B., and Mandel, J.P. (2002). Advances in understanding of fragile X pathogenesis and FMRP function, and in identification of X linked mental retardation genes. Curr. Opin. Genet. Dev. *12*, 284–293.

Bardoni, B., Schenk, A., and Mandel, J.L. (1999). A novel RNA-binding nuclear protein that interacts with the fragile X mental retardation protein. Hum. Mol. Genet. *8*, 2557–2566.

Bardoni, B., Castets, M., Huot, M.E., Schenk, A., Adinolfi, S., Corbin, F., Pastore, A., Kandjian, E.W., and Mandel, J.L. (2003). 82-FIP, a novel FMRP (fragile X mental retardation protein) interacting protein, shows a cell cycle-dependent intracellular localisation. Hum. Mol. Genet. *15*, 1689–1698.

Bartels, C., Xia, T.H., Billeter, M., Gunter, P., and Wűthrich, K. (1995). The program XEASY for computer supported NMR spectral analysis of biological macromolecules. J. Biomol. NMR *5*, 1–10.

Brown, V., Jin, P., Ceman, S., Darnell, J.C., O'Donnell, W.T., Tenenbaum, S.A., Jin, X., Feng, Y., Wilkinson, K.D., Keene, J.D., et al. (2001). Microarray identification of FMRP-associated brain mRNAs and altered mRNA translational profiles in Fragile X Syndrome. Cell *107*, 477–487.

Caudy, A.A., Myers, M., Hannon, G.J., and Hammond, S.M. (2002). Fragile X related protein and VIG associate with the RNA interference machinery. Genes Dev. *16*, 2491–2496.

Ceman, S., Brown, V., and Warren, S.T. (1999). Isolation of an FMRP associated messenger ribonucleoprotein particle and identification of nucleolin and the fragile X-related protein as components of the complex. Mol. Cell. Biol. *19*, 7925–7932.

Ceman, S., Nelson, R., and Warren, S.T. (2000). Identification of mouse YB1/p50 as a component of the FMRP-associated mRNP particle. Biochem. Biophys. Res. Commun. *279*, 904–908.

Chen, L., Yun, S.W., Seto, J., Liu, W., and Toth, M. (2003). The fragile X mental retardation protein binds and regulates a novel class of mRNAs containing U rich targets. Neuroscience *120*, 1005–1017.

Cornilescu, G., Delaglio, F., and Bax, A. (1999). Protein backbone angle restraints from searching a database for chemical shift and sequence homology. J. Biomol. NMR *13*, 289–302.

D'Agata, V., Warren, S.T., Zhao, W., Torre, E.R., Alkon, D.L., and Cavallaro, S. (2002). Gene expression profiles in a transgenic animal model of fragile X syndrome. Neurobiol. Dis. *10*, 211–218.

Darnell, J.C., Jensen, K.B., Jin, P., Brown, V., Warren, S.T., and Darnell, R.B. (2001). Fragile X Mental Retardation protein targets G quartet mRNAs important for neuronal function. Cell *107*, 489–499.

De Diego Otero, Y., Severijnen, L.-A., van Cappellen, G., Schrier, M., Oostra, B., and Willemsen, R. (2002). Transport of Fragile X Mental Retardation protein via granules in neurites of PC12 cells. Mol. Cell. Biol. *22*, 8332–8341.

Delaglio, F., Grzesiek, S., Vuister, G.V., Zhu, G., Pfeifer, J., and Bax, A. (1995). NMRPipe: a multidimensional spectral processing system based on UNIX pipes. J. Biomol. NMR *6*, 277–293.

Devys, D., Lutz, Y., Rouyer, N., Belloq, J.P., and Mandel, J.L. (1993). The FMR-1 protein is cytoplasmatic and appears normal in carriers of a fragile X premutation. Nat. Genet. *4*, 335–340.

Guntert, P., Mumenthaler, C., and Wuthrich, K. (1997). Torsion angle dynamics for NMR structure calculation with the new program DYANA. J. Mol. Biol. *273*, 283–298.

Ishizuka, A., Siomi, M.C., and Siomi, H. (2002). A *Drosophila* fragile X protein interacts with components of RNAi and ribosomal proteins. Genes Dev. *16*, 2497–2508.

Jin, P., and Warren, S.T. (2003). New insights into fragile X syndrome: from molecules to neurobehaviours. Trends Biochem. Sci. *28*, 152–158.

Kay, L.E., Nicholson, L.K., Delaglio, F., Bax, A., and Torchia, D.A. (1992). Pulse sequences for removal of the effects of cross-correlation between dipolar and chemical shift anisotropy relaxation mechanisms on the measureament of heteronuclear T1 and T2 values in proteins. J. Magn. Reson. *97*, 359–375.

Keene, J.D., and Tenenbaum, S.A. (2002). Eukaryotic mRNPs may represent post-transcriptional operons. Mol. Cell *9*, 1161–1167.

Khandjian, E.W. (1999). Biology of the fragile X mental retardation protein, an RNA-binding protein. Biochem. Cell Biol. *77*, 331–342.

Laggerbauer, B., Ostareck, D., Keidel, E.M., Ostareck-Lederer, A., and Fischer, U. (2001). Evidence that fragile X mental retardation protein is a negative regulator of translation. Hum. Mol. Genet. *10*, 329–338.

Laskowski, R.A., Rullman, J.A.C., MacArthur, M.W., Kaptein, R., and Thornton, J.M. (1996). AQUA and PROCHECK-NMR: programs for checking the quality of protein structures solved by NMR. J. Biomol. NMR *8*, 477–486.

Lefebvre, S., Burlet, P., Viollet, L., Bertrandy, S., Huber, C., Belser, C., and Munnich, A. (2002). A novel association of the SMN protein with two major non-ribosomal nucleolar proteins and its implication in spinal muscular atrophy. Hum. Mol. Genet. *11*, 1017–1027.

Li, Z., Zhang, Y., Ku, L., Wilkinson, K.D., Warren, S.T., and Feng, Y. (2001). The fragile X mental retardation protein inhibits translation via interacting with mRNA. Nucleic Acids Res. *29*, 2276–2283.

Lipari, G., and Szabo, G. (1982). A model-free approach to the interpretation of nuclear magnetic resonance relaxation in macromolecules. J. Am. Chem. Soc. *104*, 4546–4559.

Lodi, P.J., Ernst, J.A., Kuszewski, J., Hickman, A.B., Engelman, A., Craigie, R., Clore, G.M., and Gronenborn, A.M. (1995). Solution structure of the DNA binding domain of HIV-1 integrase. Biochemistry *34*, 9826–9833.

Maciejewski, M.W., Liu, D., Prasad, R., Wilson, S.H., and Mullen, G.P. (2000). Backbone dynamics and refined solution structure of the N-terminal domain of DNA polymerase β. Correlation with DNA binding and dRP lyase activity. J. Mol. Biol. *296*, 229–253.

Maurer-Stroh, S., Dickens, N.J., Hughes-Davies, L., Kouzarides, T., Eisenhaber, F., and Ponting, C.P. (2003). The Tudor domain 'Royal Family': Tudor, Plant Agenet, Chromo, PWWP and MBT domains. Trends Biochem. Sci. *28*, 69–74.

Mazroui, R., Huot, M.E., Tremblay, S., Filion, C., Label, Y., and Khandjian, E.W. (2002). Trapping of messenger mRNA by Fragile X Mental retardation protein into cytoplasmatic granules induce translational repression. Hum. Mol. Genet. *11*, 3007–3017.

Nielsen, P.R., Nietlispach, D., Mott, H.R., Callaghan, J., Bannister, A., Kouzarides, T., Murzin, A.G., Murzina, N.V., and Laue, E.D. (2002). Structure of the HP1 chromodoman bound to histone H3 methylated at lysine 9. Nature *416*, 103–107.

Otting, G., and Wuethrich, K. (1989). Extended heteronuclear editing of 2D ^{1}H NMR spectra of isotope-labeled proteins, using the X(ω_1,ω_2) double half filter. J. Magn. Reson. *85*, 586–594.

Piotto, M., Saudek, V., and Sklenar, V. (1992). Gradient-tailored excitation for single-quantum NMR spectroscopy of aqueus solutions. J. Biomol. NMR *2*, 661–665.

Reay, P., Yamasaki, K., Terada, T., Kuramitsu, S., Shirouzu, M., and Yokoyama, S. (2004). Structural and sequence comparisons arising from the solution structure of the transcription elongation factor NusG from *Thermus thermophilus*. Proteins *56*, 40–51.

Schaeffer, C., Bardoni, B., Mandel, J.L., Ehresmann, B., Ehresmann, C., and Moine, H. (2001). The Fragile X Mental Retardation protein binds specifically to its mRNA via a purine quartet motif. EMBO J. *20*, 4803–4813.

Schmidt-Zachmann, M.S., and Nigg, E.A. (1993). Protein localisation to the nucleolus: a search for targeting domains in nucleolin. J. Cell Sci. *105*, 799–806.

Schwieters, C.D., Kuszewski, J.J., Tjandra, N., and Clore, G.M. (2003). The XplorNIH NMR molecular structure determination package. J. Magn. Reson. *160*, 65–73.

Selenko, P., Sprangers, R., Stier, G., Buehler, D., Fischer, U., and Sattler, M. (2001). SMN Tudor domain structure and its interaction with SM proteins. Nat. Struct. Biol. *8*, 27–33.

Sittler, A., Devys, D., Weber, C., and Mandel, J.L. (1996). Alternative splicing of exon 14 determines nuclear or cytoplasmatic localisation of fmr1 protein isoforms. Hum. Mol. Genet. *5*, 95–102.

Sprangers, R., Groves, M.R., Sinning, I., and Sattler, M. (2003). High-resolution X-ray and NMR structures of the SMN Tudor domain: conformational variation in the binding site for symmetrically dimethylated arginine residues. J. Mol. Biol. *327*, 507–520.

Spronk, C.A., Linge, J.P., Hilbers, C.W., and Vuister, G.W. (2002). Improving the quality of protein structures derived by NMR spectroscopy. J. Biomol. NMR *22*, 281–289.

Vriend, G. (1990). WHATIF: a molecular modelling and drug design program. J. Mol. Graph. *8*, 52–56.

Vuister, G.W., and Bax, A. (1993). Quantitative J correlation: a new approach for measuring homonuclear three-bond J($H^N H^\alpha$) coupling constants in ^{15}N-enriched proteins. J. Am. Chem. Soc. *115*, 7772–7777.

Willemsen, R., Bontekoe, C., Tamanini, F., Galjaard, H., Hoogeveen, A., and Oostra, B. (1996). Association of FMRP with ribosomal precursor particles in the nucleolus. Biochem. Biophys. Res. Commun. *225*, 27–33.

Zalfa, F., Goirgi, M., Primerano, B., Moro, A., Di Penta, A., Reis, S., Oostra, B., and Bagni, C. (2003). The fragile X syndrome protein FMRP associates with BC1 RNA and regulates the translation of specific mRNAs at synapses. Cell *112*, 317–327.

Zhang, Y.Q., Bailey, A.M., Matthies, H.J., Renden, R.B., Smith, M.A., Speese, S.D., Rubin, G.M., and Broadie, K. (2001). *Drosophila* fragile X-related gene regulates the MAP1B homolog Futsch to control synaptic structure and function. Cell *107*, 591–603.

Accession Numbers

Coordinates have been deposited in the Protein Data Bank with accession code 2bkd.